Translational Oncology 14 (2021) 101065

Contents lists available at ScienceDirect

Translational Oncology

journal homepage: www.elsevier.com/locate/tranon

Construction of a prognostic immune signature for lower grade glioma that can be recognized by MRI radiomics features to predict survival in LGG patients

Zi-zhuo Li [a], Peng-fei Liu [b,*], Ting-ting An [a], Hai-chao Yang [a], Wei Zhang [a], Jia-xu Wang [a]

[a] Department of Abdominal Ultrasound, The First Affiliated Hospital of Harbin Medical University China
[b] Department of Magnetic Resonance, The First Affiliated Hospital of Harbin Medical University China

ARTICLE INFO

Keywords:
Lower grade glioma (LGG)
Immunotherapy
Radiomic
Immune-checkpoints
Neural networks

ABSTRACT

Background: This study aimed to identify a series of prognostically relevant immune features by immunophenoscore. Immune features were explored using MRI radiomics features to prediction the overall survival (OS) of lower-grade glioma (LGG) patients and their response to immune checkpoints.

Method: LGG data were retrieved from TCGA and categorized into training and internal validation datasets. Patients attending the First Affiliated Hospital of Harbin Medical University were included in an external validation cohort. An immunophenoscore-based signature was built to predict malignant potential and response to immune checkpoint inhibitors in LGG patients. In addition, a deep learning neural network prediction model was built for validation of the immunophenoscore-based signature.

Results: Immunophenotype-associated mRNA signatures (IMriskScore) for outcome prediction and ICB therapeutic effects in LGG patients were constructed. Deep learning of neural networks based on radiomics showed that MRI radiomic features determined IMriskScore. Enrichment analysis and ssGSEA correlation analysis were performed. Mutations in CIC significantly improved the prognosis of patients in the high IMriskScore group. Therefore, CIC is a potential therapeutic target for patients in the high IMriskScore group. Moreover, IMriskScore is an independent risk factor that can be used clinically to predict LGG patient outcomes.

Conclusions: The IMriskScore model consisting of a sets of biomarkers, can independently predict the prognosis of LGG patients and provides a basis for the development of personalized immunotherapy strategies. In addition, IMriskScore features were predicted by MRI radiomics using a deep learning approach using neural networks. Therefore, they can be used for the prognosis of LGG patients.

Introduction

Lower grade glioma (LGG) is a common malignant tumor originating from the central nervous system, with significant tumor heterogeneity [1,2]. Despite recent research efforts to improve prognosis of patients with LGG, half of LGG patients present with highly aggressive, drug-resistant glioma [3]. Therefore, further studies should be carried out to provide personalized therapies to improve the prognosis and treatment of LGG patients.

Tumor microenvironment is biologically important in tumors [4]. Several promising immunotherapeutic options including active or passive immunotherapy, immune checkpoint inhibitors and gene therapy have been explored for tumor treatment. These approaches significantly improve LGG treatment and show that immunotherapy plays a significant role in the treatment of LGG [5]. Recent studies report that immune genes can be used as prognostic markers to help in risk stratification and to predict of clinical outcomes in breast, gastric, thyroid and ovarian cancers [6–9]. Therefore, characteristics of genes in the tumor microenvironment play a key role in assessing patient prognosis and immunotherapy efficacy. In addition, the discovery of potential biomarkers is becoming increasingly important for the diagnosis and treatment of neurological disorders, as shown in a series of recent studies [10–14]. However, previous risk models are mainly based on a few defined gene sets. They can assess patient prognosis but are weak

Abbreviations: CIC, Capicua; CS, Conditional Survival; GO, Gene Ontology; GSEA, Gene-set Enrichment Analysis; GSVA, Gene Set Variation Analysis for Microarray and RNA-Seq data; ICB, Immune checkpoint blockade; ICI, Immune checkpoint inhibitor; KEGG, Kyoto Encyclopedia of Genes and Genomes; K-M, Kruskal-Wallis; LGG, lower grade glioma; MHC, Major histocompatibility complex; OS, Overall Survival; PCA, Principal component analysis; PFS, Progression Free Survival; qPCR, Quantitative Real-time PCR; ROC, Receiver Operating Characteristic Curve; SMC, Significantly mutated count; TCGA, The Cancer Genome Atlas.

* Corresponding author.
E-mail address: pflmedicaldoctor@163.com (P.-f. Liu).

https://doi.org/10.1016/j.tranon.2021.101065
Received 25 December 2020; Received in revised form 25 February 2021; Accepted 2 March 2021

in predicting efficacy of immunotherapy efficacy in patients [15]. Immunophenoscore, an excellent molecular marker of immune response, is used to explore the immune landscape and assess immunotherapy efficacy [16]. The scoring scheme for Immunophenoscore was based on four clusters of immune-related gene sets as previous research. These included major histocompatibility complex (MHC)-related molecules, checkpoints or immunomodulators, effector cells, and suppressor cells. A sample-wise z score from gene expression data was calculated for each gene set. Weighted average Z score was then calculated by averaging Z scores within the respective category resulting in four values. Further, the sum of weighted averaged Z scores of the four categories was computed. This protocol has been used in several studies to evaluate efficacy of immunotherapy in LGG patients, effectively predicting their response [16,17].

Magnetic resonance imaging (MRI) is widely used in the preoperative examination of LGG due to its non-invasive nature, and to explore its differentiation, providing important information for clinical diagnosis [18,19]. Several studies have explored radiomics in recent years as it provides information on the underlying pathophysiology of diseases [20,21]. Radiomics is widely used for tumor diagnosis, prognosis prediction, and selection of diagnostic and treatment approaches [22–24]. Currently, several studies on mechanistic learning approach show that radiomics is effective in the differentiation of tumors [25]. Therefore, the new MRI-based radiomics will accurately classify biomarkers identified as relevant to LGG immunotherapy and prognosis and provide information for clinical decision making. This study aimed to identify a series of prognostic immune features of LGG based on MRI radiomics features. The findings of the study provide information of response of LGG patients to immune checkpoint inhibitors and predict clinical prognosis of LGG patients. Our study hypothesizes that this approach will achieve a more intuitive and precise assessment of gliomas to aid in developing personalized therapies for LGG patients.

Methods

Data collection and patients

Data on clinical features, somatic mutation characteristics, and RNA-seq expression of low-grade glioma were retrieved from the TCGA database (https://portal.gdc.cancer.gov/). A total of 704 female patients with RNA-seq expression profiles, survival information, somatic mutation information, and common clinicopathological features were included in this study. All patients enrolled in this study were grouped into two datasets (test set and the training set) based on a 7:3 ratio. In addition, radiomics database expression data from 72 LGG patients were retrieved from TCIA database and used as a training set for radiomics-based deep learning prediction model. Furthermore, clinicopathologic and MRI imaging information of 53 patients who visited The First Affiliated Hospital of Harbin Medical University between June 2017 and June 2020 were obtained. Further, survival data and disease characteristics from clinical follow-up and medical history of these patients were obtained. Informed consent was signed by all patients included in the study signed informed consent following the Declaration of Helsinki principles. The Ethics Committee of Harbin Medical University provided ethical approval for this study. Patient inclusion criteria were: (1) patients preparing for surgery for LGG; (2) patients who underwent MRI enhancement scans within 15 days before surgery; (3) patients diagnosed with LGG by histology and immunohistochemistry; and (4) patients whose clinical and pathologic information was available. Exclusion criteria included (1) history of preoperative imatinib use, (2) patients with unknown diagnosis, and (3) patients without clinical, pathologic, and MRI imaging information. All included clinical patients were grouped in the test group to construction a deep learning predictive model based on radiomics.

Quantification of immunotherapy response predictor: immunophenoscore

Cancer antigenomes and intratumoral immune landscapes were determined by Immunophenoscore (a superior immune response molecular marker). The scoring scheme for Immunophenoscore was created based on four clusters of immune-related genomes including major histocompatibility complex (MHC)-related molecules, checkpoints or immunomodulators, effector cells, and suppressor cells. Sample *Z*-scores were retrieved and computed from gene expression data for each category. Weighted average Z-score was calculated by averaging *Z*-scores within each category to four values, and then weighting the *Z*-scores within the four categories together to obtain the final Immunophenoscore.

Identification of Immunophenoscore-associated mRNAs

Immunophenoscore of each LGG patients from TCGA were calculated for identification of immunophenoscore-associated mRNAs in LGG. Patients were then ranked in increasing order based on the level of immunophenoscore. The top 25% of patients were grouped in high immunophenoscore group, whereas the last 25% of patients were grouped in low immunophenoscore group. Expression profiles of mRNAs were compared between low and high immunophenoscore groups using microarray significance analysis. Differentially expressed mRNAs were defined as immunophenoscore-associated mRNAs (fold change > 1.0 and adjusted p Value < 0.05).

Validation of immunotherapy response

Tumour Immune Dysfunction and Exclusion (TIDE) algorithm was used to assess the clinical efficacy of immune checkpoint inhibitors [26,27]. Immunophenoscore was used to predict immune response, and validation of the result by TIDE confirmed the reliability of the immunophenoscore. Fold changes of all immune checkpoint blockade (ICB) response features in this study were log2 transformed and z transformation was applied for all features.

Construction of immune cell signatures with ssGSEA

Single-sample gene set enrichment analysis (ssGSEA) was used to evaluate relative infiltration of immune cells in LGG tumour microenvironment and the immune subpopulation gene panel [16,28,29]. The relative abundance of each immune cell type was expressed as enrichment score in ssGSEA analysis. ssGSEA scores for each immune cell type were normalized, and immune cell biosimilarity was assessed.

Identification of significantly mutated genes

MutSigCV algorithm was used to identify significantly mutant genes (SMGs). MutSigCV measured the enrichment of non-silent mutations in a gene by resolving mutation-specific background mutation rates. Statistical significance was set at $P < 0.05$.

GSEA analysis

RMA of the affy R package was used to correct and normalize TCGA-LGG expression data [30]. Limma R package was then used to assess differential expression of genes in high and low riskScore samples. Gene set enrichment analysis (GSEA) was performed using MSigDB database (v7.1) with the algorithm in bioconductor R package fgsea according to the logFC generated as input of limma package [31].

Real-time PCR

Mini-BEST Universal RNA Extraction Kit (TaKaRa, Kyoto, Japan) was used to extract total RNA according to the manufacturer's instructions as described in a previous study [32]. qPCR (PCR LightCycler480, Roche Diagnostics Ltd., Basel, Switzerland) assay was performed using SYBR Green Master Mix (TaKaRa). β-actin was used as internal control, and each sample was run five times.

Clinical MRI imaging acquisition

Clinical MRI images were acquired from First Affiliated Hospital of Harbin Medical University. Patients were instructed not to move their head during the scan to limit the potential effects of head movement. Imaging protocols include unenhanced fast T1-weighted spin-echo (T1W), fast T2-weighted spin-echo with fat suppression, and T2-weighted axial FLAIR sequences. Contrast-enhanced T1-weighted fast-filled echo sequences (or Philips) or 3DT1W-weighted magnetic preparations of fast-acquisition gradient echo sequences (on Siemens) were performed after administration of gadolinium-based contrast agent (0.1 mmol/kg body weight). Two authors manually segmented all tumor ROIs on FLAIR images based on the double-blind principle [33–35]. The entire tumor was plotted on FLAIR images based on multimodal brain tumor image segmentation benchmark, the skull was dissected using FSL library, and segmentation was performed using ITKSNAP software (http://www.itksnap.org).PyRadiomics was then used to extract radiomics features from MRI images [36]. A total of 17,722 radiomics features were extracted for each column of the radiomics imaging.

Neural network construction

PyTorch module in Python (version 3.6) was used to construct neural network models. Immunotherapy response (immunophenoscore-associated riskScore described in this study) was characteristically predicted using Linux based on radiomics features [37]. The model was set up using a random gradient descent method with the optimizer setting the learning rate at 0.001. The discard rate was set at 0.2 for each layer during training, and ReLU was set as the activation function. The neural network model was trained based on radiomics features in the TCGA-LGG cohort and tested based on radiomics features in the clinical cohort.

Statistical analysis

Euclidean distances and Ward's linkage method were used to perform Hierarchical cluster analyses. The relationship between expression levels of Immunophenophenoscore-associated mRNAs and overall survival was evaluated by univariate and multivariate Cox proportional hazard regression analysis. An Immunophenoscore-derived mRNA risk score (IMriskScore) was then constructed for prognostic prediction as follows:

$$IMriskScore = \log\left[\sum_{i=1}^{n} coef(mRNA_i) * \exp r(mRNA_i)\right],$$

Patients were categorized into high GILncSig risk and low-risk groups based on the IMriskScore in the training set.

Survival curves were calculated by the Kaplan-Meier method, and survival differences were assessed by log-rank test when considered statistical significance was observed ($p < 0.05$). Multivariate Cox regression and stratified analysis were used to assess the correlation between IMriskScore and other key clinical factors. In addition, receiver operating characteristic (ROC) curves were used to assess model performance.

Results

Identification of immunophenotype-associated mRNAs in LGG patients

Immunophenoscore was calculated for each patient and sorted in decreasing order to identify immunophenotype-associated mRNAs in LGG patients. The first 25% and the last 25% of patients were grouped in the high and low immune phenotype groups, respectively (Fig. 1A). The average immunophenoscore for immune cells has been calculated (mean 9.65, standard deviation 0.63). mRNA expression profiles of a total of 388 patients in the high immunophenoscore and low immunophenoscore groups were then compared, and 419 mRNAs with significant differences were obtained from 13,084 mRNAs ($|\log FC|>1$ and $p < 0.05$). Out of the 419, 247 mRNAs were upregulated whereas 172 mRNAs were downregulated in the high immunophenoscore group (supplementary Figure 1). The 419 differentially expressed mRNA sets were used for unsupervised hierarchical clustering analysis of the 692 samples from TCGA set (Fig. 1B). The samples were the clustered into two groups. Previous studies report that lncRNAs function as an integrated part of the immune phenotype [38]. A lncRNA-mRNA co-expression network was constructed with nodes for both lncRNAs and mRNAs to determine whether 419 mRNAs have potential functions with lncRNAs (Fig. 1C). LncRNAs and mRNAs are linked if they are interconnected. These results indicate that lncRNAs are extensively linked to mRNAs.

In recent years, numerous in vivo and in vitro pieces of evidence have shown that lncRNAs play important roles in a variety of biological processes [39–41]. LncRNAs aberrant expression may affect cell proliferation, tumor progression, or metastasis [42], therefore we have hypothesized that the expression of lncRNAs may be potentially associated with MRI radiomics. Also, our final findings show that the expression profile of mRNAs might be revealed by MRI radiomics, so we constructed an mRNA-lncRNA network to reveal the potential association of lncRNAs with immunophenoscore-related mRNAs. However, we did not find that the characteristics of lncRNAs were clearly revealed by MRI radiomics, but this does not negate the lack of correlation between lncRNAs expression and MRI radiomics. Although we did not perform further in-depth studies on lncRNAs, demonstrating the potential association of lncRNAs with immunophenoscore-related mRNAs may be potentially relevant for future studies.

Development of immunophenotype-associated mRNA signatures for outcome prediction

A total of 665 LGG patients from TCGA database were grouped into training set (n = 333) and test set (n = 332) by batch to further investigate the relationship between immunophenotype-associated mRNAs and prognosis. The main clinical and pathologic features are shown in Table 1. Further, the relationship between expression levels of immune phenotype-related mRNAs in the training set and OS were analyzed using univariate and multivariate Cox regression, and then screened for mRNAs associated with prognosis. Significant correlations were observed between seven genomic mutation-associated mRNAs and the prognosis of LGG patients ($P < 0.05$; Fig. 1E). Principal Component Analysis (PCA) classified the 665 into two groups based on these seven genes (Fig. 1D). An immune phenotype-related risk score (IMriskScore) for LGG was constructed based on results of multivariate COX regression analysis results using the seven risk prognosis-related genes. In the IMriskScore, METTL7B and TAFA3 had coefficients greater than 1, indicating that high expression of these genes is associated with poor prognosis. On the other hand, high expression of other mRNAs (HCN1, GABRA1, SULT4A1, RGS7BP, SLG12A5) was associated with good patient outcomes. In addition, low expression levels of HCN1, GABRA1, SULT4A1 and SLG12A5 mRNAs were observed in LGG relative to normal brain tissue, whereas METTL7B was significantly highly expressed in LGG patients ($p < 0.05$) (Supplementary Figure 2). IMriskScore was combined with various clinical characteristics (age, gender, grade, radiation,

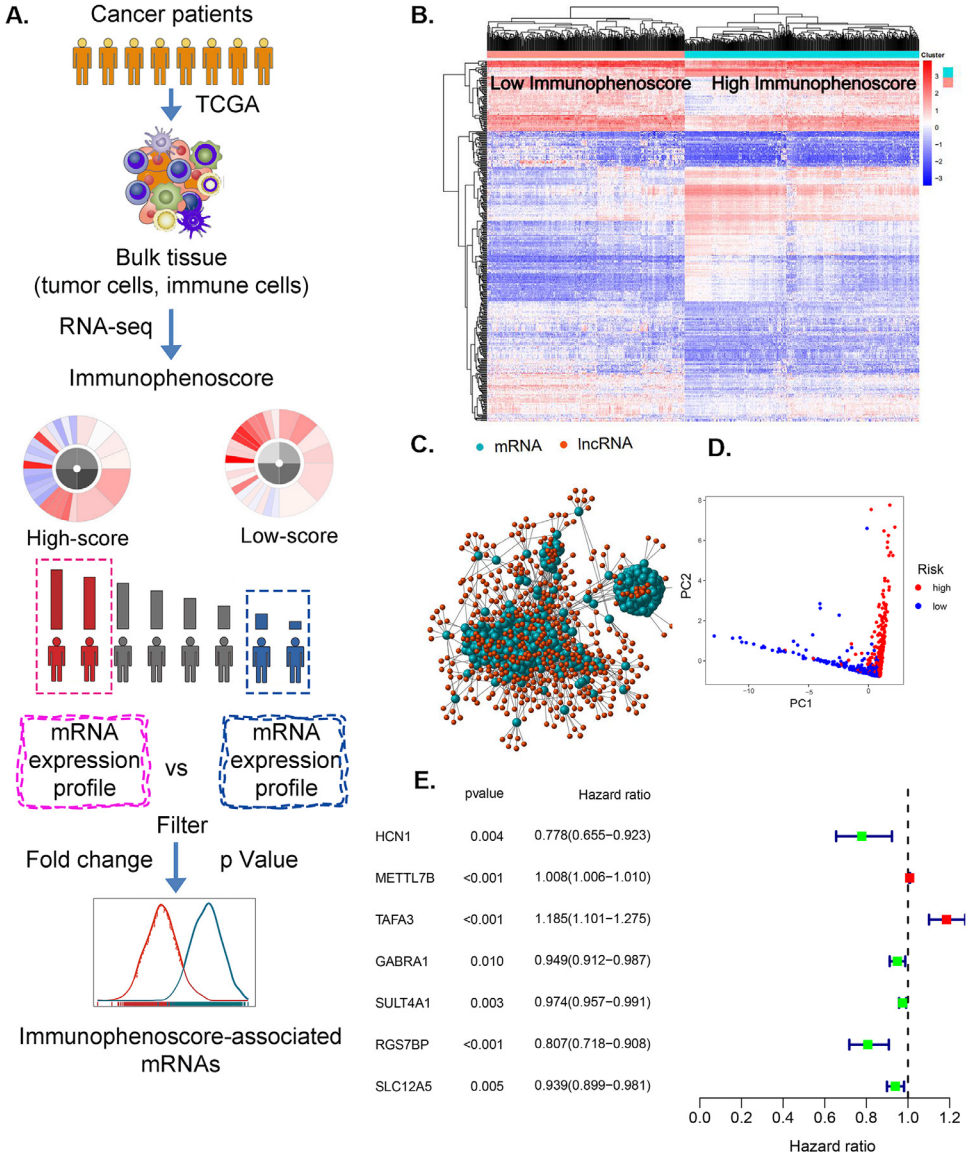

Fig. 1. Identification of immunophenoscore-associated mRNAs from LGG patients and development of IMriskScore system for outcome prediction

A. Flowchart of immunophenotype-associated mRNA identification in LGG patients. Patients were obtained from TCGA database, and mRNA expression profiles of high immunophenoscore and low immunophenoscore groups were compared by calculating the Immunophenoscore to identify immunephenotype-associated mRNAs.

B. Unsupervised clustering of 692 LGG patients based on immunephenotype-associated mRNAs. The red cluster represents low immunophenoscore, whereas the blue cluster represents high immunophenoscore group.

C. Co-expression networks of immune phenotype-associated lncRNAs and mRNAs were constructed using Pearson's correlation coefficient analysis. The red color represents lncRNAs and the blue color represents mRNAs.

D. PCA shows that TCGA LGG set can be divided into two parts based on IMriskScore-related genes. Blue dots represent higher IMriskScore ones, whereas red dots indicate the lower ones.

E. Forest chart showing mRNAs (HCN1, METTL7B, TAFA3, GABRA1, SULT4A1, RGS7BP and SLC12A5) selected from multivariate COX regression model ($p < 0.05$).

seizure, response, histological, neoadjuvant, pharmaceutical, cancer history). Multivariate COX regression analysis of IMriskScore and clinical characteristics further confirmed the clinical value of the IMriskScore. These findings show that IMriskScore is an independent prognostic factor for LGG patients (Table 2).

Validating the risk assessment capabilities of IMriskScore in LGG patients

Patients are assigned to groups with different prognostic risks based on median IMriskScore. Patients with scores below the threshold formed the low-risk group whereas patients with scores above the threshold formed the high-risk group. Survival analysis based on TCGA dataset showed than patients in the high-risk group had worse survival outcomes compared with patients in the low-risk group, both in the training and testing groups (Fig. 2A, B and Supplementary Figure 2A). The receiver operating characteristic curve (ROC) showed that IMriskScore is a good predictor of prognosis. AUC of the TCGA cohort was 0.765 whereas the test group had an AUC of 0.699 (Fig. 2C and Supplementary Fig. 2B). The predictive power of the IMriskScore for RT-PCR samples (normalized by z-score) of 56 LGG patients from the First Affiliated Hospital of Harbin Medical University was 0.705 (Fig. 2D). Clinical and pathological statistical characteristics of patients from the First Affiliated Hospital of Harbin Medical University are shown in Table 3. These finding imply that IMriskScore has potential clinical applications. Heat maps, scatter plots of overall survival (OS), and risk score distributions for the seven genes from the training and test groups are shown in Fig. 2E & F.

Correlation analysis of IMriskScore-related mRNAs

Survival analysis revealed that the expression of IMriskScore-related mRNAs (GABRA1, HCN1, METTL7B, RGS7BP, SLC12A5, SULT4A1 and TAFA3) was associated with the prognosis of LGG patients (Fig. 3A). It is these mRNAs that are positively or negatively correlated with prognosis that together form the prognostic model (IMriskScore) for LGG patients. This implies that these IMriskScore-related mRNAs can be used as prognostic markers for LGG. In addition, these IMriskScore-related mRNAs genes were significantly correlated ($p < 0.05$) with at least three immune checkpoints (Fig. 3B). Immunophenoscore, an excellent molecular marker of immune response, is used to explore the immune landscape and assess immunotherapy efficacy [16]. Immunophenoscore has been used in several studies to evaluate the efficacy of immunotherapy in LGG patients, effectively predicting their response [16,17]. IMriskScore is based on assigning immunophenoscores from bulk RNAseq

Table 1
Clinical information and pathologic features for TCGA LGG patient sets in this study.

Variables	TGGA set (n = 665)	Training set (n = 333)	Testing set (n = 332)	p-value
Age, n (%)				
≤65	578(86.92%)	287(86.19%)	291(87.65%)	0.6564
>65	87(13.08%)	46(13.81%)	41(12.35%)	
Gender, n (%)				
FEMALE	282(42.41%)	137(41.14%)	145(43.67%)	0.5602
MALE	383(57.59%)	196(58.86%)	187(56.33%)	
Grade, n (%)				
G2	245(36.84%)	117(35.14%)	128(38.55%)	0.8084
G3	260(39.1%)	128(38.44%)	132(39.76%)	
unknow	160(24.06%)	88(26.43%)	72(21.69%)	
Radiation, n (%)				
NO	118(17.74%)	64(19.22%)	54(16.27%)	0.5395
YES	143(21.5%)	71(21.32%)	72(21.69%)	
unknow	404(60.75%)	198(59.46%)	206(62.05%)	
Seizure, n (%)				
NO	175(26.32%)	91(27.33%)	84(25.3%)	0.2711
YES	298(44.81%)	138(41.44%)	160(48.19%)	
unknow	192(28.87%)	104(31.23%)	88(26.51%)	
Response, n (%)				
Complete Remission	84(12.63%)	45(13.51%)	39(11.75%)	0.7907
Partial Remission	50(7.52%)	27(8.11%)	23(6.93%)	
Progressive Disease	39(5.86%)	20(6.01%)	19(5.72%)	
Stable Disease	59(8.87%)	27(8.11%)	32(9.64%)	
unknow	433(65.11%)	214(64.26%)	219(65.96%)	
Histological, n (%)				
Astrocytoma	191(28.72%)	98(29.43%)	93(28.01%)	0.2592
Glioblastoma Multiforme (GBM)	1(0.15%)	0(0%)	1(0.3%)	
Oligoastrocytoma	128(19.25%)	66(19.82%)	62(18.67%)	
Oligodendroglioma	187(28.12%)	82(24.62%)	105(31.63%)	
Treated primary GBM	1(0.15%)	1(0.3%)	0(0%)	
Untreated primary GBM	157(23.61%)	86(25.83%)	71(21.39%)	
Neoadjuvant, n (%)				
No	662(99.55%)	332(99.7%)	330(99.4%)	0.9979
YES	3(0.45%)	1(0.3%)	2(0.6%)	
History with LGG, n (%)				
NO	154(23.16%)	83(24.92%)	71(21.39%)	0.4854
YES	5(0.75%)	4(1.2%)	1(0.3%)	
unknow	506(76.09%)	246(73.87%)	260(78.31%)	

Table 2
Univariate and multivariate Cox regression analyses of IMriskScore with Clinical information and pathologic features.

	Univariate Cox regression analyses				Multivariate Cox regression analyses			
Variable	HR	lower 95%Cl	upper 95%Cl	p value	HR	lower 95%Cl	upper 95%Cl	p value
Training set								
age	1.078	1.053	1.104	0.000	1.082	1.054	1.111	0.000
gender	1.077	0.615	1.886	0.796				
grade	5.334	2.658	10.706	0.000	4.308	2.034	9.124	0.000
seizure	0.954	0.540	1.685	0.872				
histological	0.604	0.428	0.855	0.004	0.707	0.501	0.998	0.049
riskScore	1.727	1.437	2.076	0.000	1.432	1.134	1.809	0.003
Testing set								
age	1.067	1.050	1.084	0.000	1.070	1.051	1.089	0.000
gender	0.971	0.657	1.434	0.882				
grade	3.004	1.965	4.593	0.000	2.053	1.311	3.217	0.002
seizure	0.748	0.505	1.106	0.146				
histological	0.725	0.577	0.912	0.006	0.717	0.565	0.910	0.006
riskScore	1.595	1.327	1.919	0.000	1.377	1.102	1.722	0.005

samples. Therefore, we hypothesize that the IMriskScore is related to immunotherapy.

Previous studies report that the normal expression of the IDH1 gene is closely associated with glioma development and is an important clinical marker for patient prognosis. Recent studies report that the combination of IDH1 inhibitors with chemotherapy improves the clinical prognosis of patients [43]. In neuro-oncology, the exceptional disease control demonstrated by IDH1 inhibitors was presented at the ASCO 2020 meeting, where a clinical phase II study of the IDH1 inhibitor FT-2102, in combination with azacitidine, in patients with recurrent or progressive gliomas with IDH1 mutations, achieved a 47% disease control rate and a median progression-free survival of 8.3 months [43]. Radar plots showed that IMriskScore-related mRNAs (GABRA1, HCN1, METTL7B, RGS7BP, SLC12A5, SULT4A1 and TAFA3) are significantly correlated with IDH1 (Fig. 3C). In addition, high expression of IDH1 was significantly correlated with IMriskScore ($p < 0.05$) (Fig. 3D), implying that IMriskScore may be used to assess the efficacy of IDH1-associated targeted therapies. In summary, IMriskScore-related mRNAs and IM-

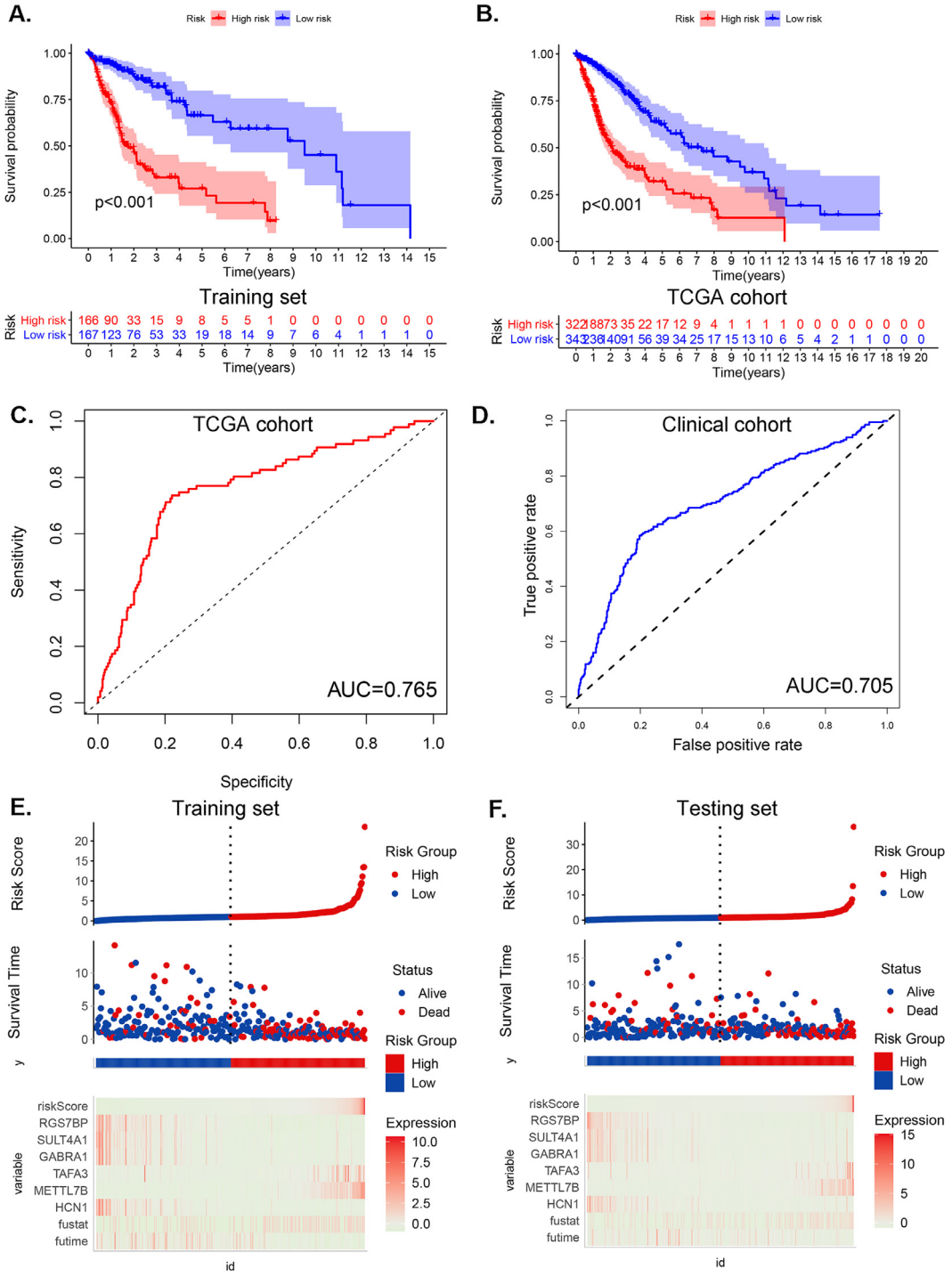

Fig. 2. Validating risk assessment capabilities of IMriskScore in LGG patients

A-B. IMriskScore signature was related to OS survival. Kaplan-Meier curves of overall survival based on IMriskScore groups in the training set (A) and TCGA cohort (B).

D. ROC for IMriskScore based on TCGA set (n= 665) (C) and Clinical set (n=56) (D).

E-F. Patients were grouped into high-IMriskScore group and low-IMriskScore group. Heatmap of 7 IMriskScore-related genes and IMriskScore curve for training set and testing set.

riskScore may sever as potential predictors of immunotherapy efficacy and chemotherapy efficacy in LGG patients.

Role of IMriskScore in immune checkpoint inhibitor treatment

IMriskScore-related mRNAs are derived from Immunophenotype-associated mRNA signatures. Therefore, we speculate that they may regulate leukocyte infiltration and immune-related pathways. Our findings showed that most of the immune checkpoints were associated with IMriskscore, and immune checkpoint or immunotherapy related mRNAs (CD23, PD-L1, CTLA4, PD1, IDO1, IFNG, IL2 and LAG3) were significantly enriched in the high IMriskScore group (Fig. 4A) (Supplementary Figure 3). CD23, IL2, LAG3, IDO1 and IFNg were chosen because their expression correlates with the immune profile of the tumour microen-

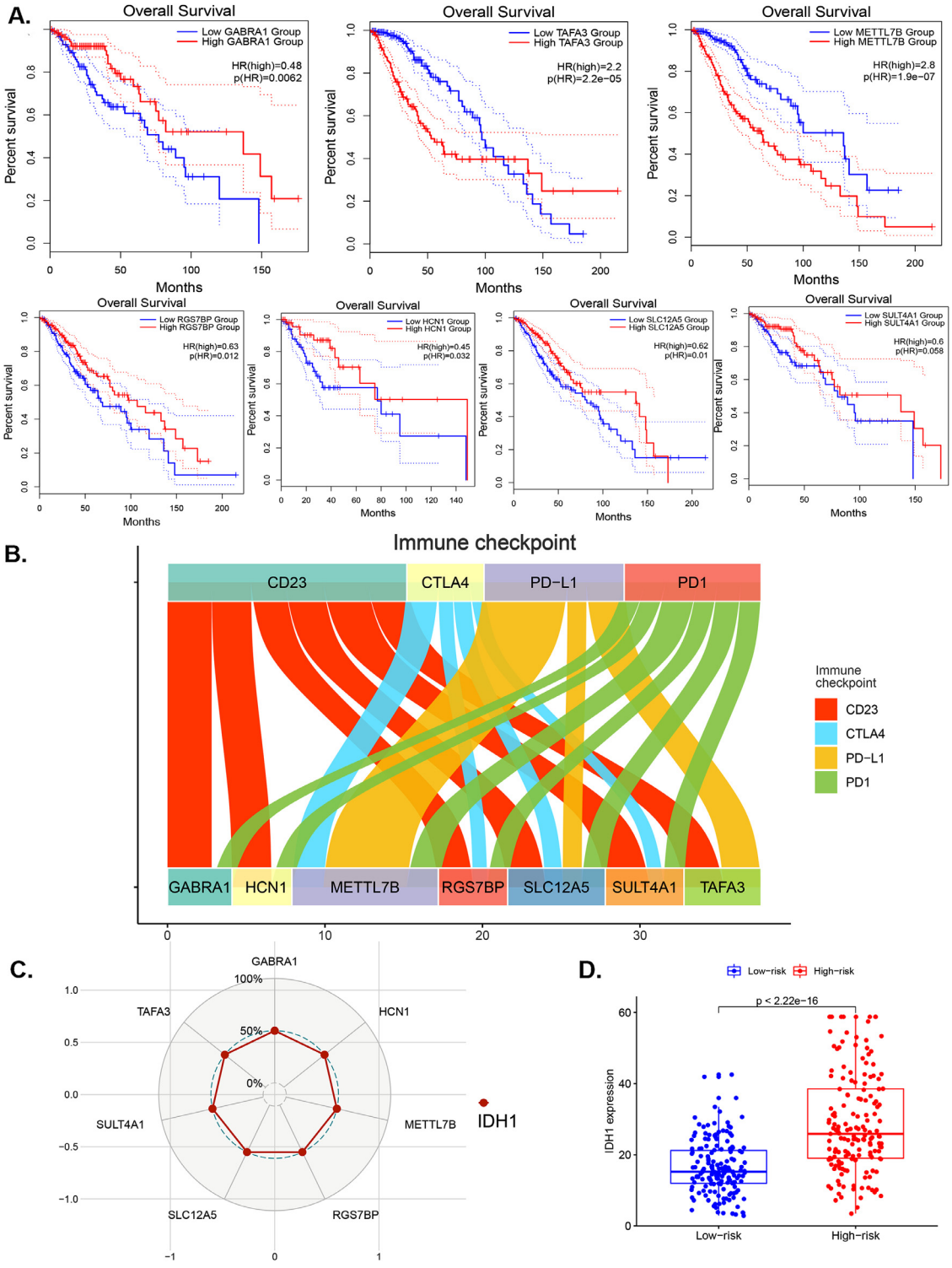

Fig. 3. Correlation analysis of IMriskScore-related mRNAs with LGG treatment checkpoints

A. K-M survival analysis of OS based on IMriskScore-related mRNAs (GABRA1, HCN1, METTL7B, RGS7BP, SLC12A5, SULT4A1 and TAFA3) in the TCGA cohort.

B. Interrelationship Network of IMriskScore-related mRNAs (GABRA1, HCN1, METTL7B, RGS7BP, SLC12A5, SULT4A1 and TAFA3) and immune checkpoints (CD23, CTLA4, PD-L1 and PD1). The width of the line represents degree of correlation.

C. Radar plots reflect interrelationship between IDH1 and mRNA, all of which were statistically significant.

D. Differential expression of IDH1 in the low- and high-IMriskScore groups (Mann-Whitney U test, $P < 0.001$).

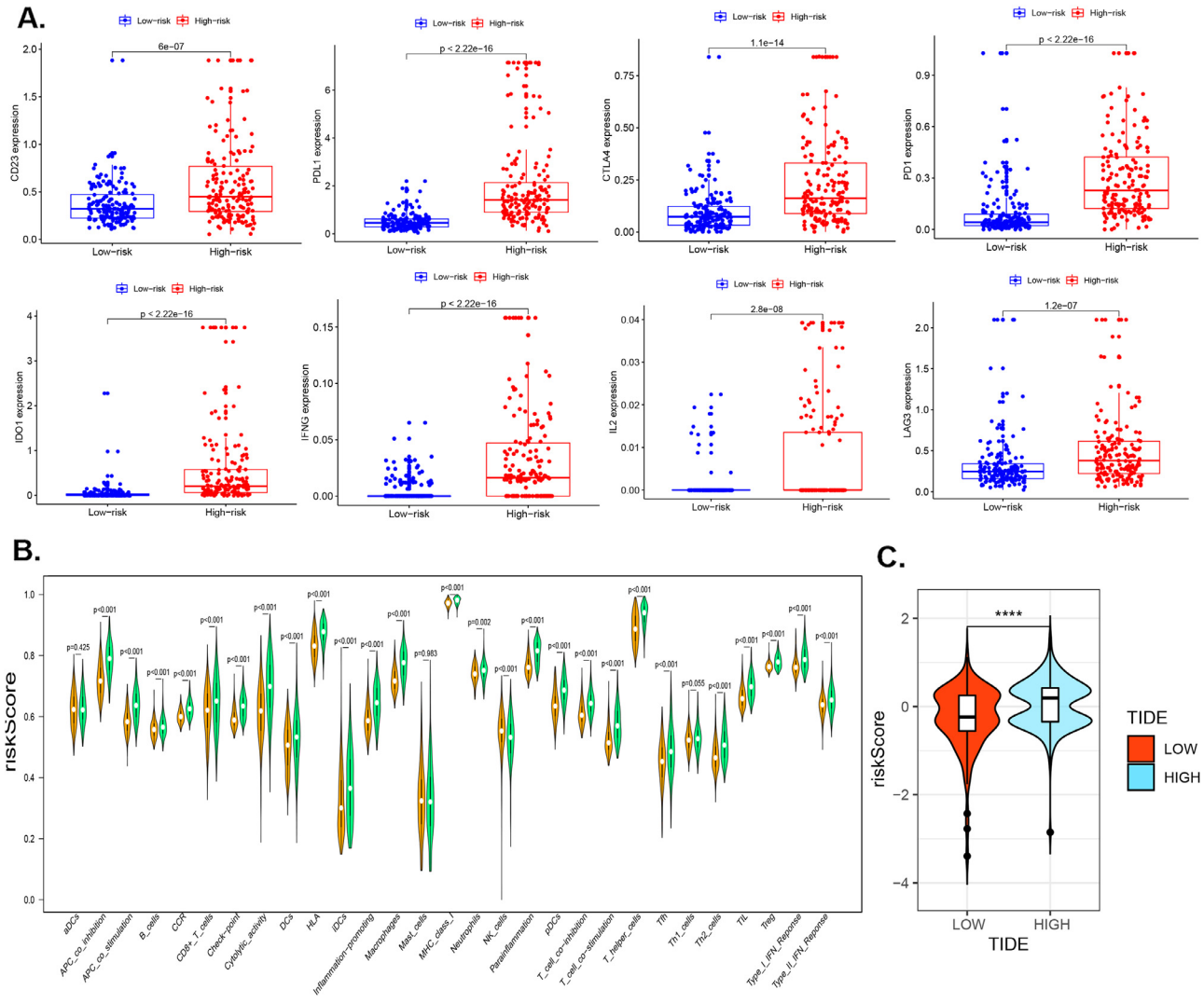

Fig. 4. Role of IMriskScore in immune checkpoint inhibitor treatment

A. Differential expression of immune checkpoint mRNAs (HCN1, METTL7B, TAFA3, GABRA1, SULT4A1, RGS7BP and SLC12A5) in the low- and high-IMriskScore groups (Mann-Whitney U test, $P < 0.001$).

Box plots were used to visualize differences in infiltration abundance of 29 immune cell subpopulations and their functions in the low and high IMriskScore groups. The high-risk group is represented in orange, whereas green represents the low-risk group.

C. TIDE score between high- and low- IMriskScore patients.

vironment. We need to clarify that CD23, IL2, LAG3, IDO1, and IFNg were chosen because their expression correlates with the immune profile of the tumor microenvironment [16,17,44]. LGG data from TCGA database was used to construct a set of box plots to visualize the relative abundance of 29 immune infiltrating cell subpopulations and functions (Fig. 4B). Low expression levels of APC co-inhibition, APC co-stimulation, B cells, CCR, CD8+ T cell, checkpoint, cytolytic activity, DCs HLA, iDSs, inflammation-promoting, macrophages, MHC class I, neutrophils, NK cells, parainflammation, pDCs, T cell co-inhibition, T cell co-stimulation, T helper cells, Tfh, Th2 cells, TIL, Treg, Type I IFN Reponse and Type II IFN Reponse, were observed in the low-risk group ($P < 0.05$). The TIDE score has been validated by numerous studies as an innovative prognostic assessment protocol for immune checkpoint suppression therapy. Furthermore, the TIDE algorithm was used to validate the predictive power of IMriskScore for immunotherapy. Interestingly, we found that immunotherapy was more effective in the high IMriskScore risk group compared to the low IMriskScore group (Fig. 4C). Therefore, these findings imply that IMriskScore is associated with tumor immunotherapy.

Identification of significantly mutant genes with IMriskScore

A somatic mutation count (SMC) analysis was performed based on LGG samples from the low IMriskScore and high IMriskScore groups. A lower proportion of SMCs was found in the low IMriskScore group compared with the high IMriskScore group. This finding explains high levels of immune infiltration in the high IMriskScore group (Fig. 5A). Higher SMCs are more likely to attract immune cell infiltration resulting in immune enrichment. In addition, this finding implies that the high IMriskScore group is more likely to achieve better outcomes from immunotherapeutic [45]. UBQLN4 is a newly discovered gene associated with genomic instability. Expression levels of UBQLN4 were compared between high IMriskScore and low IMriskScore groups. Expression of UBQLN4 in the high IMriskScore group was significantly lower com-

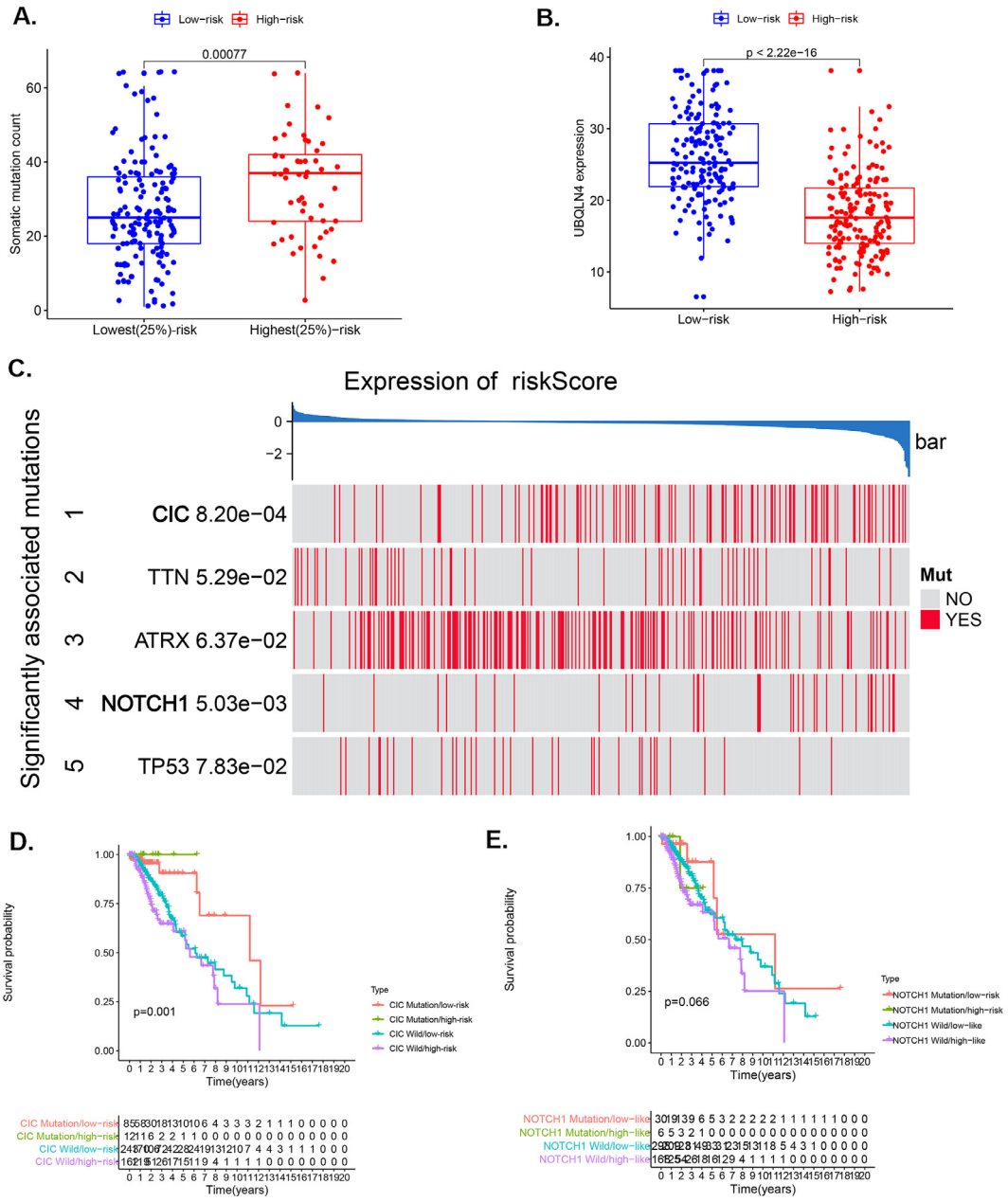

Fig. 5. Identification of significantly mutant genes with IMriskScore

A-B. Differential somatic mutation count in the low- and high-IMriskScore groups (A); Differential expression of genetic instability driver gene UBQLN4 in the low- and high-IMriskScore groups (B) (Mann-Whitney U test, $P < 0.001$).

C. Waterfall plots of mutation frequency difference genes based on low- and high-risk component strata acquired in the TCGA LGG cohort.

D. K-M estimates of OS of patients with CIC mutation or CIC wild in low- or high risk predicted by the IMriskScore.

E. K-M estimates of OS of patients with NOTCH1 mutation or NOTCH1 wild in low- or high risk predicted based on IMriskScore.

pared with expression level in the low IMriskScore group (Fig. 5B). This implies that IMriskScore is correlated with genetic instability. Further, a waterfall plot was constructed for genes with different mutation frequencies between high and low-risk groups (Fig. 5C). A significant lower mutation frequency of Capicua (CIC) and NOTCH1 was observed in the low-IMriskScores group compared with the high-risk group. Survival analysis show that CIC mutations are associated with a better prognosis, whereas NOTCH1 mutations do not have a significant effect on prognosis compared with CIC mutations (Fig. 5D-E). In summary, IMriskScores are significantly associated with LGG gene instability, whereas CIC mutations in high-risk patients are associated with a better prognosis. This implies that mutations in the CIC gene correlate with the IMriskScore and may be an important risk marker for glioma prognosis.

Functional characterization of IMriskScore subtypes

GO function analysis of GSEA showed enrichment of IMriskScore-related signaling functions including: negative regulation of humoral immune response, positive regulation of fibroblast proliferation, and programmed cell death involved in cell development re-

Table 3
Clinical information and pathologic features for clinical cohort.

Variables	Alive (n = 39)	Dead (n = 17)	Total (n = 56)	p-value
Risk				
high	12 (30.77)	7 (41.18)	19 (33.93)	0.449
low	27 (69.23)	10 (58.82)	37 (66.07)	
Follow-up time (day)	513±628	1084±1209	687±877	0.08
Age				
<=65	38 (97.44)	13 (76.47)	51 (91.07)	0.011*
>65	1 (2.56)	4 (23.53)	5 (8.93)	
Gender				
FEMALE	20 (51.28)	11 (64.71)	31 (55.36)	0.353
MALE	19 (48.72)	6 (35.29)	25 (44.64)	
Grade				
G2	15 (38.46)	4 (23.53)	19 (33.93)	0.278
G3	24 (61.54)	13 (76.47)	37 (66.07)	
Histological				
Astrocytoma	12 (30.77)	7 (41.18)	19 (33.93)	0.636
Oligoastrocytoma	11 (28.21)	3 (17.65)	14 (25.00)	
Oligodendroglioma	16 (41.03)	7 (41.18)	23 (41.07)	

* $p<0.05$ ** $p<0.01$

sponse interleukin-2 and Wnt signaling pathway involved in midbrain dopaminergic neuron (Fig. 6A). Furthermore, KEGG pathways analysis of GSEA showed enrichment of IMriskScore-related pathways (including allograft rejection, apoptosis-multiple species, HIF-1 signaling pathway, Nicotine addiction, as well as Synthesis and degradation of ketone bodies) (Fig. 6B). Enrichment of these biological functions and pathways implies that IMriskScore can predict LGG tumor-immune interaction in the tumor microenvironment.

Independence of the IMriskScore from other clinical factors and clinical application

Determination of conditional survival (CS) is necessary for cancers with poor survival prognosis. In this study, the 6-year postoperative survival rate in the low IMriskScore group (58%) was more than twice as high as that of the high IMriskScore group (26%). Patients in the low IMriskScore group showed higher survival rates at 1–3 years after surgery than those in the high IMriskScore group (Fig. 7A & B). Survival rates of patients who survived for more than 3 years in both groups were similar in the following years. This implies that IMriskScore is a good predictor of patient survival between the first and the third year after surgery. Therefore, IMriskScore can predict poor prognosis within three years after surgery, enabling clinicians to provide targeted care. Survival analysis showed that IMriskscore was a good predictor across age and gender (Fig. 7C-F). These results imply that IMriskScore has broad clinical application.

IMriskScore evaluated by preclinical mri-based deep learning model

A neural network-based deep learning model was constructed to predict IMriskScore based on MRI radiomics features (Fig. 8A). Predictions based on radiomics showed that patients in the high-risk group had a lower survival rate than those in the low-risk group (Fig. 8B). Patients at lower risk were more likely to be predicted in the low IMriskScore risk group by the imagingomics deep learning model (Fig. 8C). A total of 68 patients from the TCGA LGG cohort with MRI radiomics information were included as a training group for neural network-based deep learning, and 56 patients from the First Affiliated Hospital of Harbin Medical University were used as a test group for neural network-based deep learning. AUC value of the ROC curve was 0.821 in the test group (Fig. 8D) and 0.708 in the test group after carrying out 1000 training sessions (Fig. 8E, Table 4). All samples were correctly identified using the confusion matrix as shown in Fig. 8F-H. This finding implies that the Preclinical MRI-based Deep Learning Model is better in assessing IMriskScore. Therefore, the IMriskScore has wide clinical application as a scoring system that can be recognized by MRI radiomics.

Discussion

Despite recent significant advances in treatment and diagnosis of LGG, most LGG patients have poor prognosis [46]. Although neoadjuvant immune checkpoint blockade (ICB) therapy improves overall prognosis of patients, immunotherapy for gliomas is now in clinical trials with slow progress [47–49]. Advances on studies on molecular mechanisms of immunity, have achieved precision cancer treatment for a variety of cancers [50,51]. However, no effective immune-related molecular markers have yet been identified for accurate prognosis and treatment of LGG [52]. Therefore, more studies should be conducted to identify biomarkers to prediction the effectiveness of immunotherapy in LGG patients.

To address these shortcomings of current therapies, we first developed an LGG immunotherapy efficacy and OS prognostic risk prediction model that can be recognized by MRI radiomics. The IMriskScore was shown to be significantly correlated with prognosis, CIC mutations, and immunotherapy efficacy in LGG patients and showed that MRI radiomics-based prediction models can accurately predict IMriskScore in patients with LGG. IMriskScore based on seven characteristic mRNAs (HCN1, METTL7B, TAFA3, GABRA1, SULT4A1, RGS7BP, SLC12A5) was significantly correlated with OS in LGG patients. Similar results were obtained from the clinical sample, whereby patients in the low IMriskScore group showed a better prognosis than those in the high IMriskScore group. Stratified analysis showed that the IMriskScore was effective in predicting overall survival regardless of clinical presentation. A prognostic evaluation of the overall survival of LGG patients using the IMriskScore showed that the 5-year survival rate after treatment was approximately 62% in the low IMriskScore group, compared with 32% in the high IMriskScore group. However, patients who survived for than 3 years, showed similar survival rates in both groups. Therefore, the survival rate of both groups of patients gradually stabilized over time and CS rate increased. In addition, IMriskScore can identify high-risk patients, help individualize the probability of survival, help patients cope with the fear of recurrence or the risk of death, and inform on individualized follow-up time [53–55].

The seven mRNAs used to construct IMriskScore (GABRA1, HCN1, METTL7B, RGS7BP, SLC12A5, SULT4A1, TAFA3), most of which have been elucidated in several studies, are potential prognostic-related markers for LGG. Previous studies report that GABAAR is associated with clinical features correlated with poor prognosis in LGG patients (including seizures, memory impairment, hallucinations and anxiety) [56]. HCN1 and METTL7B are driver-related genes for glioma [57]. A previous study reports that SLC12A5 and SULT4A1 are associated with neural-related tumor prognosis [58]. TAFA3 is a novel secreted protein that modulates microglial/macrophage polarization dynamics and affects local blood supply [59]. Therefore, TAFA3 may serve as an important immune function in the glioma tumor microenvironment. Although previous studies report that RGS7BP is implicated in pathogenesis of clinical diseases such as epilepsy, more studies should be carried out to explore the role of RGS7BP in glioma [60]. In summary, the seven IMriskScore-related genes identified in our study are associated with OS prognosis in LGG patients.

Tumor microenvironment and immune cells play key roles in tumor prognosis [61]. Enrichment analysis showed that IMriskScore is associated with immune-related functions or pathways, such as programmed cell. This is because IMriskScore system is based on immunophenoscore, which has been shown in numerous studies to be a superior predictor of ICB treatment [16]. Programmed cell death 1 (PD-1) is an immune checkpoint receptor expressed on activated T and B cells and binds to programmed cell death 1 ligand 1 (PD-L1), which inhibits T cell proliferation and activation. The binding of PD-1 to PD-L1 allows cancer cells to more effectively evade immune attack in the tumor microenvironment

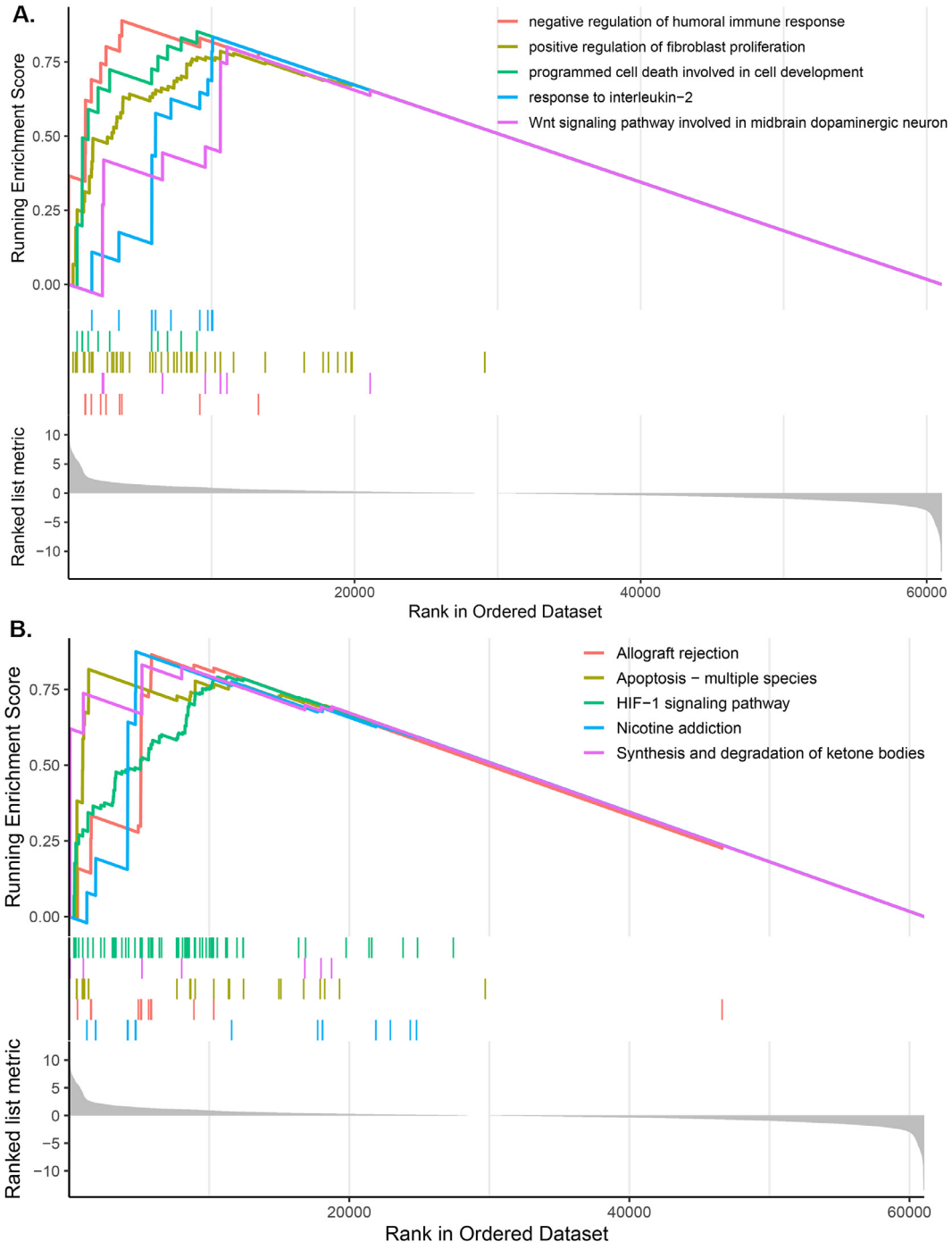

Fig. 6. Functional characterization of IMriskScore subtypes

GSEA showing KEGG pathway analysis and GO function analysis of pathways and functions associated with IMriskScore. Significant correlations were observed between high and low IMriskScore expression groups.

A. GO enrichment analysis.

B. KEGG enrichment analysis

Table 4

AUC comparison test for ROC curves.

Groups	AUC	SE	95% CI	Sensitivity	Specificity	*p value*
Training set	0.821	0.642	0.704–0.938	0.773	0.87	0.2508
Testing set	0.708	0.078	0.556–0.861	0.579	0.838	

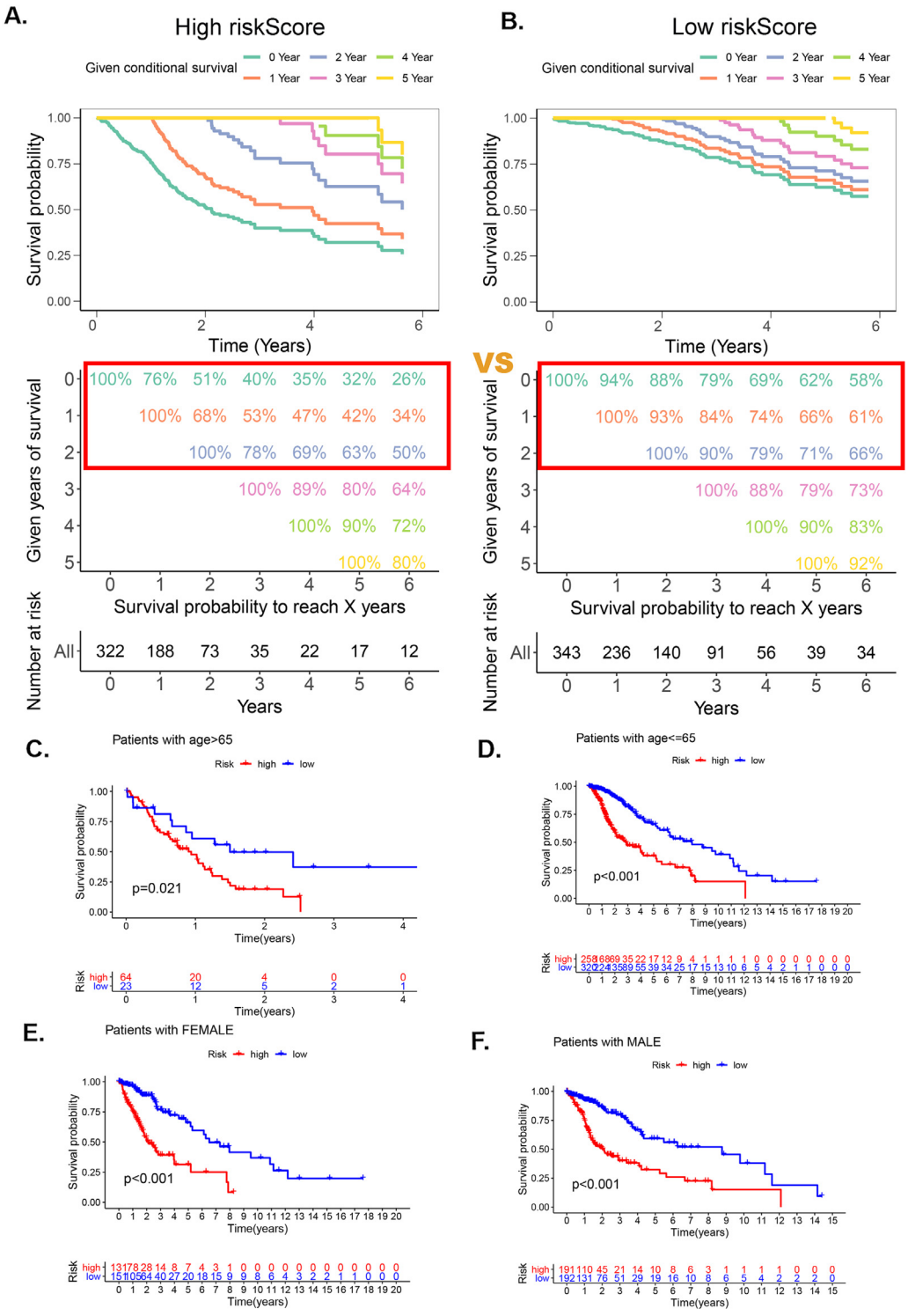

Fig. 7. Independence of IMriskScore from other clinical factors and clinical application.
A-B. Estimated survival rates of patients given a 0–5 year-survival period in low/high-BCPRS groups. Each column represents years of survival and each row represents the percentage of attaining a certain total survival time from the survived years point;
C-F. K-M of OS based on the clinical characteristic.

[62–64]. PD-1 antibodies can be used to effectively treat a variety of cancers and improve OS [65,66]. Immune checkpoints and T-cells were enriched on the high IMriskScore group. This implies that in highly malignant LGGs, immune cells do not fully exert their immune anticancer effects despite their high degree of infiltration [44]. In addition, TIDE prediction shows a more optimistic response to immunotherapy in the high IMriskScore group, which is consistent with immunophenoscore results. Therefore, the IMriskScore model can be used as a reliable predictive tool to guide LGG immune-related therapy.

Luchini et al. report that MSC and immune checkpoint expression are essential for immune checkpoint inhibition therapy [67]. Previous studies report that an increase in MSC is positively associated with higher

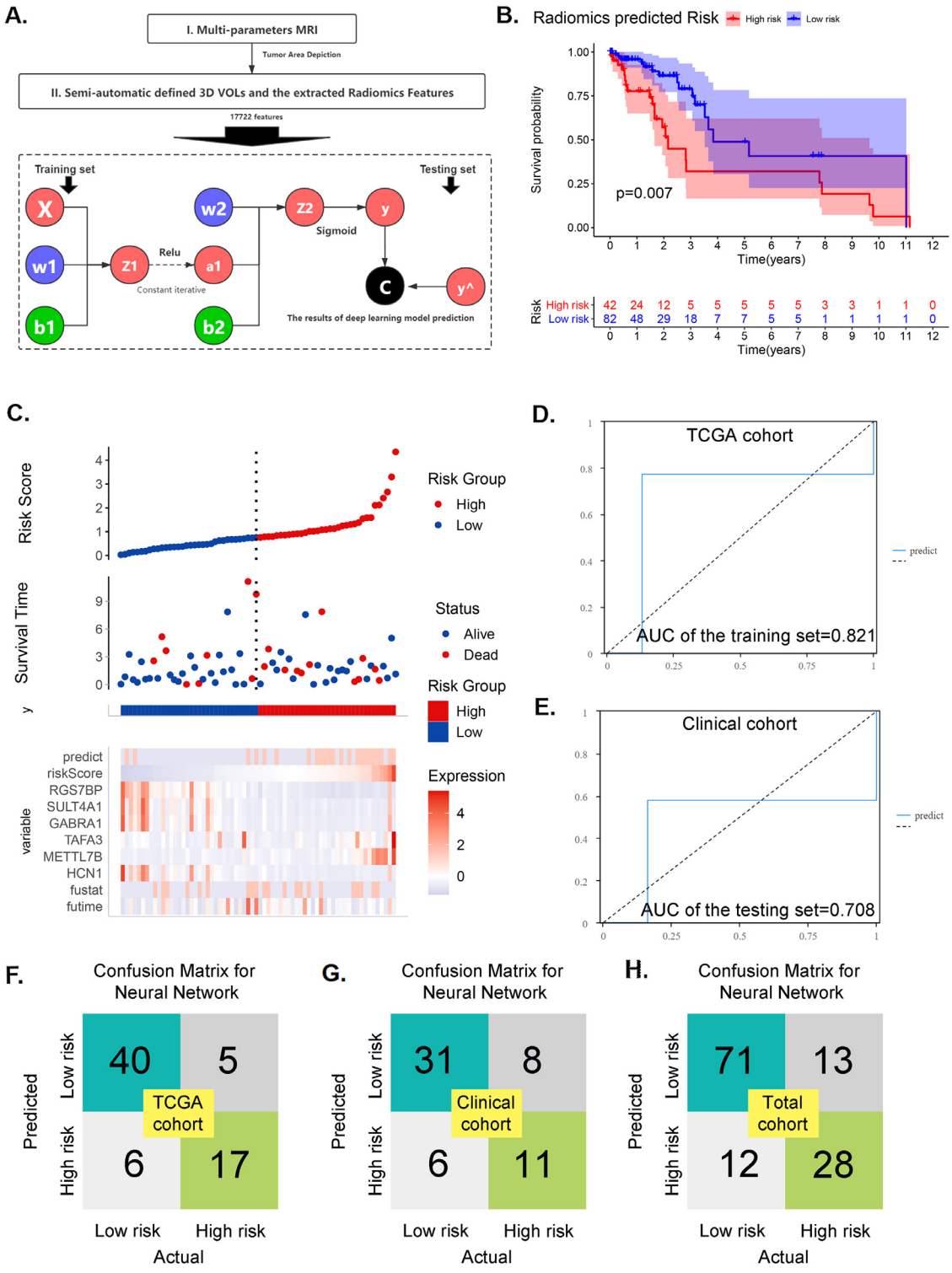

Fig. 8. IMriskScore evaluated by preclinical MRI-based deep learning model

A. TCGA cohort was used as a test group, whereas the clinical cohort was used as a training group.

B. K-M of OS based on radiomics predicted risk in the TCGA cohort.

C. Heatmap of 7 IMriskScore-related genes and IMriskScore curve. Patients at lower risk were more likely to be predicted in the low IMriskScore risk group by the imagingomics deep learning model.

D-E. Receiver operating characteristic curve for preclinical MRI-based deep learning model based on the training set (TCGA cohort) (C) and the testing set (clinical cohort) (D).

F-H. Confusion matrix for deep learning models of neural networks. TCGA cohort (F); Clinical cohort (G); total cohort (H).

survival [68]. In this study, MSC was higher in the low IMriskScore group, implying a potential correlation between IMriskScore and genetic instability. In addition, CIC, a frequently mutated gene in LGG, showed a considerably higher mutation rate in the low IMriskScore group [69]. Interestingly, CIC mutations in the high IMriskScore group were associated with approximately 100% survival rate. Previous studies report that capicua (CIC) is an intrinsic negative immune regulator of cells [70]. The absence of CIC promotes helper T cell differentiation and immune response [71]. Therefore, a high IMriskScore score may be an indicator of good prognosis in patients with CIC mutations. We propose for the first time that CIC mutations are an important prognostic factor in LGG and may be associated with efficacy of immunotherapy. A high IMriskScore may suggest a poor prognosis for CIC wild-type patients, whereas a high IMriskScore may suggest a positive prognosis for CIC mutant patients. This implies that the use of CIC's targeted agents for patients with high IMriskScore may significantly improve the prognosis of patients.

Radiomics can extract hundreds of quantitative features from medical images and effectively predict tumor-related biological behavior [72–74]. In diffuse low-grade gliomas, MRI radiomics models have been shown to predict IDH mutations and tumor aggressiveness [75]. Previous studies report that MRI radiomics features of gliomas can be used to predict the grade of glioma [25]. And CIC mutations also can be accurately identified by MRI radiomics in LGG patients, as seen in previous studies [76]. Previous papers have focused on the association of MRI radiomics with specific genes/prognosis. Although the role of gene sets has become increasingly appreciated in recent years, especially in oncology studies [77], the association of MRI radiomics with gene sets remains unexplored. In this study, we found that IMriskScore features can be predicted using MRI radiomics through neural network-based deep learning, which shows potential clinical application. IMriskScore is a series of genetic markers associated with an immune score. This study, therefore, suggests that MRI radiomics may have the potential to predict specific genetic markers.

Radiomics characteristics of LGG were retrieved from TCGA database and clinical patients, and used to construct a neural network-based deep learning model to predict IMriskScore of patients. This radiomic-based IMriskScore was used to predict efficacy and prognosis of tumor immunotherapy from MRI image data. A deep learning approach was used to assess radiomics features of IMriskScore and tumor immune microenvironment features of LGG. The model showed good classification accuracy. The model showed good predictive ability in both TCGA cohort and clinical cohort, with an AUC value of 0.821. The confusion matrix indicated that the method has a potential for clinical application. A series of immunophenotype-associated mRNAs in LGG patients were identified in this study. Further, the study presents immunophenotype-associated mRNA signatures (IMriskScore) for outcome prediction and ICB therapeutic effects, and validates ability of IMriskScore to assess prognostic risk in LGG patients. Radiomics-based deep learning in neural networks showed that IMriskScore can be predicted using MRI radiomic features. Enrichment analysis and ssGSEA correlation analysis showed that IMriskScore was significantly correlated with immunotherapy-related immune checkpoints and immune microenvironment. High-frequency mutant CIC, an immunosuppressive gene, showed a high mutation frequency in the low IMriskScore group. CIC mutation is significantly correlated with a good outcome of patients in the high IMriskScore group. Therefore, CIC is a potential therapeutic target for patients in the high IMriskScore group. Finally, the IMriskScore shows a wide clinical application as an independent predictor. The findings of this study provide information for predicting the effects of immunotherapy and the prognosis of LGG patients. However further studies should be carried out to validate the findings of this study. First, since immunotherapy is not yet widely available in many developing countries, it is difficult to obtain information on the efficacy of immunotherapy directly from clinical settings. Here, we proposed a new method to overcome this difficulty. This approach is to use the immunophenoscore to obtain a scoring system for the efficacy of immunotherapy and then use TIDE to investigate the predictive power of this scoring system, which we believe has scientific applications. However, the model still requires further clinical case validation. In addition, further clinical studies are needed to explore the combined effect of IMriskScore and CIC mutations on efficacy of immunotherapy and prognosis of LGG patients. Finally, although a new cohort was used to validate the radiomics-based neural network deep learning IMriskScore prediction model, the sample size was small and more patients from multiple centers should be included to confirm the generalizability of the model.

Conclusion

In conclusion, the IMriskScore model an independent feature for assessing the prognosis of LGG patients provides basis for development of personalised immunotherapy development. Mutations in the high-frequency mutant gene CIC are associated with IMriskScore and significantly affect the prognosis of LGG patients. IMriskScore features can be predicted using MRI radiomics through neural network-based deep learning, which shows potential clinical application.

Declaration of Competing Interest

No competing interests exist.

Acknowledgements

We thank the anonymous reviewers for their valuable comments and suggestions that helped improve the quality of this manuscript.

Funding

No.

Ethics approval and consent to participate

Informed written consent was obtained from all patients included in this study. This study was approved by the Institutional Ethics Review Board of the First Affiliated Hospital of Harbin Medical University.

Author contributions

Zi-zhuo Li: Conceptualization, Methodology, Software, Data curation, Writing- Original draft preparation, Visualization, Investigation, Validation.

Peng-fei Liu:, Conceptualization, Methodology, Software, Data curation, Writing- Reviewing and Editing, Visualization, Investigation, Validation.

Ting-ting An: Methodology, Software, Data curation.

Hai-chao Yang: Methodology, Software, Data curation.

Wei Zhang: Visualization, Investigation, Validation.

Jia-xu Wang: Investigation, Validation.

All authors read and approved the final manuscript.

Data availability

The datasets generated and analyzed during the present study are available in supplementary materials.

Supplementary materials

Supplementary material associated with this article can be found, in the online version, at doi:10.1016/j.tranon.2021.101065.

References

[1] Q.T. Ostrom, H. Gittleman, P. Farah, A. Ondracek, Y. Chen, Y. Wolinsky, et al., CBTRUS statistical report: Primary brain and central nervous system tumors diagnosed in the United States in 2006-2010, Neuro. Oncol. 15 (Suppl 2) (2013) ii1–i56.

[2] W.J. Zeng, Y.L. Yang, Z.Z. Liu, Z.P. Wen, Y.H. Chen, X.L. Hu, et al., Integrative analysis of DNA methylation and gene expression identify a three-gene signature for predicting prognosis in lower-grade gliomas, Cell Physiol. Biochem. 47 (2018) 428–439.

[3] E.B. Claus, K.M. Walsh, J.K. Wiencke, A.M. Molinaro, J.L. Wiemels, J.M. Schildkraut, et al., Survival and low-grade glioma: the emergence of genetic information, Neurosurg. Focus 38 (2015) E6.

[4] D. Hanahan, R.A. Weinberg, Hallmarks of cancer: the next generation, Cell 144 (2011) 646–674.

[5] H. Mahmoodzadeh Hosseini, R. Halabian, M. Amin, A.A. Imani Fooladi, Texosome-based drug delivery system for cancer therapy: from past to present, Cancer Biol. Med. 12 (2015) 150–162.

[6] M.L. Ascierto, M. Kmieciak, M.O. Idowu, R. Manjili, Y. Zhao, M. Grimes, et al., A signature of immune function genes associated with recurrence-free survival in breast cancer patients, Breast Cancer Res. Treat. 131 (2012) 871–880.

[7] K. Kim, S. Jeon, T.M. Kim, C.K. Jung, Immune gene signature delineates a subclass of papillary thyroid cancer with unfavorable clinical outcomes, Cancers (Basel) (2018) 10.

[8] S. Shen, G. Wang, R. Zhang, Y. Zhao, H. Yu, Y. Wei, et al., Development and validation of an immune gene-set based Prognostic signature in ovarian cancer, EBioMedicine 40 (2019) 318–326.

[9] W. Yang, Z. Lai, Y. Li, J. Mu, M. Yang, J. Xie, et al., Immune signature profiling identified prognostic factors for gastric cancer, Chin J. Cancer Res. 31 (2019) 463–470.

[10] Y. Chen, L. Liang, S. Cao, G. Hou, Q. Zhang, H. Ma, et al., Serum CCL21 as a potential biomarker for cognitive impairment in spinal cord injury, Biomed Res. Int. 2020 (2020) 6692802.

[11] Imaging Hyperreflective Foci as an Inflammatory Biomarker after Anti-VEGF Treatment in Neovascular Age-Related Macular Degeneration Patients with Optical Coherence Tomography Angiography.

[12] L. Kui, Z. Zhang, Y. Wang, Y. Zhang, S. Li, X. Dong, et al., Genome assembly and analyses of the macrofungus macrocybe gigantea, Biomed. Res. Int. 2021 (2021) 6656365.

[13] M. Xu, X.Y. He, P. Huang, The relationship between the mean platelet volume and carotid atherosclerosis and prognosis in patients with acute cerebral infarction, Biomed. Res. Int. 2020 (2020) 6685740.

[14] X. Wang, F. Zhang, W. Ma, D. Feng, J. Zhang, J. Xu, Increased levels of serum neuregulin 1 associated with cognitive impairment in vascular dementia, Biomed. Res. Int. 2020 (2020) 6683747.

[15] M. Zhang, X. Wang, X. Chen, Q. Zhang, J. Hong, Novel immune-related gene signature for risk stratification and prognosis of survival in lower-grade glioma, Front. Genet 11 (2020) 363.

[16] P. Charoentong, F. Finotello, M. Angelova, C. Mayer, M. Efremova, D. Rieder, et al., Pan-cancer immunogenomic analyses reveal genotype-immunophenotype relationships and predictors of response to checkpoint blockade, Cell Rep. 18 (2017) 248–262.

[17] X. Li, D. Wen, X. Li, C. Yao, W. Chong, H. Chen, Identification of an immune signature predicting prognosis risk and lymphocyte infiltration in colon cancer, Front. Immunol. 11 (2020) 1678.

[18] M. Kimura, L.C.H. da Cruz Jr., Multiparametric MR imaging in the assessment of brain tumors, Magn. Reson. Imaging Clin. N Am. 24 (2016) 87–122.

[19] S. Abrol, A. Kotrotsou, A. Salem, P.O. Zinn, R.R. Colen, Radiomic phenotyping in brain cancer to unravel hidden information in medical images, Top Magn. Reson Imaging 26 (2017) 43–53.

[20] P. Lambin, E. Rios-Velazquez, R. Leijenaar, S. Carvalho, R.G. van Stiphout, P. Granton, et al., Radiomics: extracting more information from medical images using advanced feature analysis, Eur. J. Cancer 48 (2012) 441–446.

[21] P. Prasanna, J. Patel, S. Partovi, A. Madabhushi, P. Tiwari, Erratum to: Radiomic features from the peritumoral brain parenchyma on treatment-naïve multi-parametric MR imaging predict long versus short-term survival in glioblastoma multiforme: Preliminary findings, Eur. Radiol. 27 (2017) 4198–4199.

[22] P. Kickingereder, M. Götz, J. Muschelli, A. Wick, U. Neuberger, R.T. Shinohara, et al., Large-scale radiomic profiling of recurrent glioblastoma identifies an imaging predictor for stratifying anti-angiogenic treatment response, Clin. Cancer Res. 22 (2016) 5765–5771.

[23] E. Sala, E. Mema, Y. Himoto, H. Veeraraghavan, J.D. Brenton, A. Snyder, et al., Unravelling tumour heterogeneity using next-generation imaging: radiomics, radiogenomics, and habitat imaging, Clin. Radiol. 72 (2017) 3–10.

[24] Y. Li, X. Liu, K. Xu, Z. Qian, K. Wang, X. Fan, et al., MRI features can predict EGFR expression in lower grade gliomas: a voxel-based radiomic analysis, Eur. Radiol. 28 (2018) 356–362.

[25] Q. Wang, Q. Li, R. Mi, H. Ye, H. Zhang, B. Chen, et al., Radiomics nomogram building from multiparametric MRI to predict grade in patients with glioma: a cohort study, J Magn. Reson Imaging 49 (2019) 825–833.

[26] F. Xu, H. Zhang, J. Chen, L. Lin, Y. Chen, Immune signature of T follicular helper cells predicts clinical prognostic and therapeutic impact in lung squamous cell carcinoma, Int. Immunopharmacol. 81 (2020) 105932.

[27] F. Xu, X. Zhan, X. Zheng, H. Xu, Y. Li, X. Huang, et al., A signature of immune-related gene pairs predicts oncologic outcomes and response to immunotherapy in lung adenocarcinoma, Genomics 112 (2020) 4675–4683.

[28] Q. Jia, W. Wu, Y. Wang, P.B. Alexander, C. Sun, Z. Gong, et al., Local mutational diversity drives intratumoral immune heterogeneity in non-small cell lung cancer, Nat. Commun. 9 (2018) 5361.

[29] D.A. Barbie, P. Tamayo, J.S. Boehm, S.Y. Kim, S.E. Moody, I.F. Dunn, et al., Systematic RNA interference reveals that oncogenic KRAS-driven cancers require TBK1, Nature 462 (2009) 108–112.

[30] M.E. Ritchie, B. Phipson, D. Wu, Y. Hu, C.W. Law, W. Shi, et al., limma powers differential expression analyses for RNA-sequencing and microarray studies, Nucleic Acids Res 43 (2015) e47.

[31] A. Subramanian, P. Tamayo, V.K. Mootha, S. Mukherjee, B.L. Ebert, M.A. Gillette, et al., Gene set enrichment analysis: a knowledge-based approach for interpreting genome-wide expression profiles, Proc. Natl. Acad. Sci. U S A 102 (2005) 15545–15550.

[32] Y. Jiang, S. Han, W. Cheng, Z. Wang, A. Wu, NFAT1-regulated IL6 signalling contributes to aggressive phenotypes of glioma, Cell Commun. Signal 15 (2017) 54.

[33] M. Jenkinson, C.F. Beckmann, T.E. Behrens, M.W. Woolrich, S.M. Smith, FSL, Neuroimage 62 (2012) 782–790.

[34] B.H. Menze, A. Jakab, S. Bauer, J. Kalpathy-Cramer, K. Farahani, J. Kirby, et al., The multimodal brain tumor image segmentation benchmark (BRATS), IEEE Trans. Med. Imaging 34 (2015) 1993–2024.

[35] P.A. Yushkevich, J. Piven, H.C. Hazlett, R.G. Smith, S. Ho, J.C. Gee, et al., User-guided 3D active contour segmentation of anatomical structures: significantly improved efficiency and reliability, Neuroimage 31 (2006) 1116–1128.

[36] J.J.M. van Griethuysen, A. Fedorov, C. Parmar, A. Hosny, N. Aucoin, V. Narayan, et al., Computational radiomics system to decode the radiographic phenotype, Cancer Res. 77 (2017) e104–e1e7.

[37] A P., S G., S C., G C., E Y., Z D. Automatic Diferentiation in Pytorch. 2017.

[38] M. Wu, P. Fu, L. Qu, J. Liu, A. Lin, Long noncoding RNAs, new critical regulators in cancer immunity, Front. Oncol. 10 (2020) 550987.

[39] W.X. Peng, P. Koirala, Y.Y. Mo, LncRNA-mediated regulation of cell signaling in cancer, Oncogene 36 (2017) 5661–5667.

[40] T.R. Mercer, J.S. Mattick, Structure and function of long noncoding RNAs in epigenetic regulation, Nat. Struct. Mol. Biol. 20 (2013) 300–307.

[41] Y. Wang, Z.J. Zhao, X.R. Kang, T. Bian, Z.M. Shen, Y. Jiang, et al., lncRNA DLEU2 acts as a miR-181a sponge to regulate SEPP1 and inhibit skeletal muscle differentiation and regeneration, Aging (Albany NY) 12 (2020) 24033–24056.

[42] A. Sanchez Calle, Y. Kawamura, Y. Yamamoto, F. Takeshita, T. Ochiya, Emerging roles of long non-coding RNA in cancer, Cancer Sci 109 (2018) 2093–2100.

[43] MIDL F., H C., M R., BAV T., V M. A phase Ib/II study of olutasidenib in patients with relapsed/refractory IDH1 mutant gliomas: safety and efficacy as single agent and in combination with azacitidine. 2020; 38:2505-.

[44] F. Huemer, M. Leisch, R. Geisberger, T. Melchardt, G. Rinnerthaler, N. Zaborsky, et al., Combination strategies for immune-checkpoint blockade and response prediction by artificial intelligence, Int. J. Mol. Sci. 21 (2020).

[45] A. Desrichard, A. Snyder, T.A. Chan, Cancer neoantigens and applications for immunotherapy, Clin. Cancer Res. 22 (2016) 807–812.

[46] G. Youssef, J.J. Miller, Lower grade gliomas, Curr. Neurol. Neurosci. Rep. 20 (2020) 21.

[47] R. DA, OS10.3 randomized phase 3 study evaluating the efficacy and safety of nivolumab vs bevacizumab in patients with recurrent glioblastoma: CheckMate 143, Neuro. Oncol. 19 (2017) iii21–iiiii.

[48] T.F. Cloughesy, A.Y. Mochizuki, J.R. Orpilla, W. Hugo, A.H. Lee, T.B. Davidson, et al., Neoadjuvant anti-PD-1 immunotherapy promotes a survival benefit with intratumoral and systemic immune responses in recurrent glioblastoma, Nat. Med. 25 (2019) 477–486.

[49] K.A. Schalper, M.E. Rodriguez-Ruiz, R. Diez-Valle, A. López-Janeiro, A. Porciuncula, M.A. Idoate, et al., Neoadjuvant nivolumab modifies the tumor immune microenvironment in resectable glioblastoma, Nat. Med. 25 (2019) 470–476.

[50] G.A. McArthur, P.B. Chapman, C. Robert, J. Larkin, J.B. Haanen, R. Dummer, et al., Safety and efficacy of vemurafenib in BRAF(V600E) and BRAF(V600K) mutation–positive melanoma (BRIM-3): extended follow-up of a phase 3, randomised, open-label study, Lancet Oncol. 15 (2014) 323–332.

[51] T.C. Westbrook, I.S. Hagemann, J. Ley, K. Chen, K. Palka, J. Liu, et al., Prospective assessment of the clinical benefit of a tailored cancer gene set built on a next-generation sequencing platform in patients with recurrent or metastatic head and neck cancer, Med. Oncol. 37 (2019) 12.

[52] K. Aslan, V. Turco, J. Blobner, J.K. Sonner, A.R. Liuzzi, N.G. Núñez, et al., Heterogeneity of response to immune checkpoint blockade in hypermutated experimental gliomas, Nat. Commun. 11 (2020) 931.

[53] M. Mori, M. Fujimori, H. Ishiki, T. Nishi, J. Hamano, H. Otani, et al., Adding a wider range and "hope for the best, and prepare for the worst" statement: preferences of patients with cancer for prognostic communication, Oncologist 24 (2019) e943–ee52.

[54] B. Thewes, O. Husson, H. Poort, J.A.E. Custers, P.N. Butow, S.A. McLachlan, et al., Fear of cancer recurrence in an era of personalized medicine, J. Clin. Oncol. 35 (2017) 3275–3278.

[55] A.E.J. Latenstein, S. van Roessel, L.G.M. van der Geest, B.A. Bonsing, C.H.C. Dejong, B. Groot Koerkamp, et al., Conditional survival after resection for pancreatic cancer: a population-based study and prediction model, Ann. Surg. Oncol. 27 (2020) 2516–2524.

[56] P.I. D'Urso, O.F. D'Urso, C. Storelli, M. Mallardo, C.D. Gianfreda, A. Montinaro, et al., miR-155 is up-regulated in primary and secondary glioblastoma and promotes tumour growth by inhibiting GABA receptors, Int. J. Oncol. 41 (2012) 228–234.

[57] A. Liang, B. Zhou, W. Sun, Integrated genomic characterization of cancer genes in glioma, Cancer Cell. Int. 17 (2017) 90.

[58] Z. Sun, H. Li, X.H. Shu, H. Shi, X.Y. Chen, Q.Y. Kong, et al., Distinct sulfonation activities in resveratrol-sensitive and resveratrol-insensitive human glioblastoma cells, Febs J. 279 (2012) 2381–2392.

[59] Y. Shao, T. Deng, T. Zhang, P. Li, Y. Wang, FAM19A3, a novel secreted protein, modulates the microglia/macrophage polarization dynamics and ameliorates cerebral ischemia, FEBS Lett. 589 (2015) 467–475.
[60] M. Crippa, P. Malatesta, M.T. Bonati, F. Trapasso, F. Fortunato, G. Annesi, et al., A familial t(4;8) translocation segregates with epilepsy and migraine with aura, Ann. Clin. Transl. Neurol. 7 (2020) 855–859.
[61] F P., MAFC B., FCMF S.-C. Effffector memory T cells, Early Meta Surv. Colorectal Cancer.
[62] P. Zheng, Z. Zhou, Human cancer immunotherapy with PD-1/PD-L1 blockade, Biomark Cancer 7 (2015) 15–18.
[63] S. Lyford-Pike, S. Peng, G.D. Young, J.M. Taube, W.H. Westra, B. Akpeng, et al., Evidence for a role of the PD-1:PD-L1 pathway in immune resistance of HPV-associated head and neck squamous cell carcinoma, Cancer Res. 73 (2013) 1733–1741.
[64] Y. Yang, Cancer immunotherapy: harnessing the immune system to battle cancer, J. Clin. Invest 125 (2015) 3335–3337.
[65] T. Shukuya, D.P. Carbone, Predictive markers for the efficacy of anti-PD-1/PD-L1 antibodies in lung cancer, J. Thorac. Oncol. 11 (2016) 976–988.
[66] L. Chen, X. Han, Anti-PD-1/PD-L1 therapy of human cancer: past, present, and future, J. Clin. Invest. 125 (2015) 3384–3391.
[67] C. Luchini, F. Bibeau, M.J.L. Ligtenberg, N. Singh, A. Nottegar, T. Bosse, et al., ESMO recommendations on microsatellite instability testing for immunotherapy in cancer, and its relationship with PD-1/PD-L1 expression and tumour mutational burden: a systematic review-based approach, Ann. Oncol. 30 (2019) 1232–1243.
[68] R.J. Hause, C.C. Pritchard, J. Shendure, S.J. Salipante, Classification and characterization of microsatellite instability across 18 cancer types, Nat. Med. 22 (2016) 1342–1350.
[69] M.S. Alghamri, R. Thalla, R.P. Avvari, A. Dabaja, A. Taher, L. Zhao, et al., Tumor mutational burden predicts survival in patients with low-grade gliomas expressing mutated IDH1, Neurooncol. Adv. 2 (2020) vdaa042.
[70] J. Han, J.T. Perez, C. Chen, Y. Li, A. Benitez, M. Kandasamy, et al., Genome-wide CRISPR/Cas9 screen identifies host factors essential for influenza virus replication, Cell Rep. 23 (2018) 596–607.
[71] S. Park, S. Lee, C.G. Lee, G.Y. Park, H. Hong, J.S. Lee, et al., Capicua deficiency induces autoimmunity and promotes follicular helper T cell differentiation via derepression of ETV5, Nat Commun. 8 (2017) 16037.
[72] C. Wang, H. Li, Y. Jiaerken, P. Huang, L. Sun, F. Dong, et al., Building CT radiomics-based models for preoperatively predicting malignant potential and mitotic count of gastrointestinal stromal tumors, Transl. Oncol. 12 (2019) 1229–1236.
[73] T. Chen, Z. Ning, L. Xu, X. Feng, S. Han, H.R. Roth, et al., Radiomics nomogram for predicting the malignant potential of gastrointestinal stromal tumours preoperatively, Eur. Radiol. 29 (2019) 1074–1082.
[74] T. Chen, S. Liu, Y. Li, X. Feng, W. Xiong, X. Zhao, et al., Developed and validated a prognostic nomogram for recurrence-free survival after complete surgical resection of local primary gastrointestinal stromal tumors based on deep learning, EBioMedicine 39 (2019) 272–279.
[75] M. Kim, S.Y. Jung, J.E. Park, Y. Jo, S.Y. Park, S.J. Nam, et al., Diffusion- and perfusion-weighted MRI radiomics model may predict isocitrate dehydrogenase (IDH) mutation and tumor aggressiveness in diffuse lower grade glioma, Eur. Radiol. 30 (2020) 2142–2151.
[76] L. Zhang, F. Giuste, J.C. Vizcarra, X. Li, D. Gutman, Radiomics features predict CIC mutation status in lower grade glioma, Front. Oncol. 10 (2020) 937.
[77] M.A. Clarke, J. Fisher, Executable cancer models: successes and challenges, Nat. Rev. Cancer 20 (2020) 343–354.